Basrah Journal for Engineering Sciences, Vol. 22, No. 2, (2022), 57-64

Original Article

Journal homepage: www.bjes.edu.iq
ISSN (Online): 23118385, ISSN (Print): 18146120

OPEN ACCESS

Numerical Analysis of Slotted Wings Using Fluid-Structure Interaction

Makarim A. Hassan [1,*], Rafil M. Laftah [2], Muneer A. Ismael [3]

[1,2,3] *Department of Mechanical Engineering, College of Engineering, University of Basrah, Basrah, Iraq*
E-mail addresses: mahabs1m1@gmail.com , rafil.laftah@uobasrah.edu.iq , muneer.ismael@uobasrah.edu.iq
Received: 17 May 2022; Revised: 1 June 2022; Accepted: 8 June 2022; Published: 24 December 2022

Abstract

For shorter landing and take-off path in airports, the aircrafts should reduce their speed with keeping high lifting force. This paper is to identify solutions to increase the lift force of the wing significantly under several flight scenarios (such as takeoff and landing) using leading-edge slats and their relationship with the dynamic parameters of the aerodynamic wing. The study is performed by the use of ABAQUS 2016 software. The problem is solved for turbulent flow and 2-dimensional composite wing at constant Reynolds's number of (6.49×10^5) and constant boundary conditions. Various depths have been used for the auxiliary airfoil at constant width and gap. All stresses at the wing base were obtained. The pressure distribution on the airfoil surface was determined, air velocity distribution was tracked over the surface, lift and drag forces and their coefficients were computed. The results show that the highest value of the lift coefficient is 0.489 at the depth (-3 %) of the wing chord, it decreases when the depth of the slat becomes zero %, and the rise returns with increasing depth to (4 %), but it does not reach the maximum value, while the highest drag coefficient was (1.89) at depth (4 %) of the wing chord. The maximum value of Von Mises stress was found at depth of 4 % with value of 1.605×10^5 Pa.

Keywords: Airfoil, Clark Y-14, Lift coefficient, Drags coefficient, Slotted wing, Turbulent flow.

https://doi.org/10.33971/bjes.22.2.9

1. Introduction

For shorter landing and take-off paths in airports, the aircrafts should reduce their speed with keeping high lifting force. A slat is a moveable device attached to the wing of the airplane to increase lift force at low speeds. As cited in [1], Lachmann, Handley and Zapareka invented the slat mechanism and it became among the pioneer strategies for landing and taking off at slow speeds. The slat is a movable leading-edge device that protects against the increased danger of stalling. The wing area is increased by moving the slats forward. The design may increase drag, decreasing performance during the cruising phase of the flight. However, it generates more lift and reduces distance, and lowers required velocity for takeoff and landing. Figure 1 shows the geometric variables for the auxiliary airfoil and main wing. With the slat closed, all measurements are provided as a percentage of the main wing chord [1]. The performance of a wing is determined by a number of factors, including lift, stalling, angle of attack, and drag. Lift and drag are the two forces that operate on the wing. Computational fluid dynamics (CFD) uses numerical analysis and algorithms to solve the Navier-Stokes equations.

The performance of wings is influenced by a number of factors. Lift, angle of attack (AOA), and drag are examples of these. All these parameters are shown in Fig. 2.

The effectiveness of slats has been the subject of several studies some of these were experimental and others theoretical works.

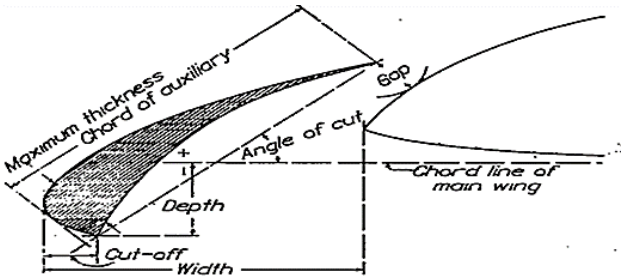

Fig. 1 Geometric variables for auxiliary airfoil [1].

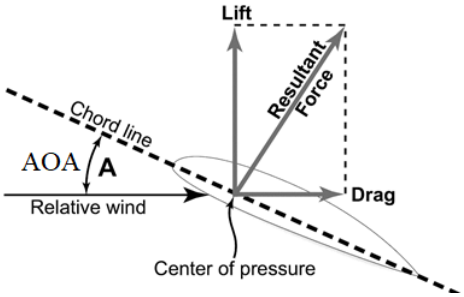

Fig. 2 the wing's aerodynamic force balances.

In 1932 Wenzinger and Shortal [1] utilized a 5-foot-diameter vertical wind tunnel (1.524 meters). A Clark Y-14 wing with slots has been tested. The wing cord measured 25.4 cm. The wind was blowing at 35 m/sec. Because the slat was tiny in size, the slat was created from aluminum alloy, while the wing was built from laminated mahogany. The experiment

considered 100 different places where the slot gap, slot width, and slot depth were altered. The slot gap ranges from 1.5 to 3.5 percent of the chord, the slot width from 3.35 to 15 percent of the chord, and the slot depth from 3.5 above to 4 percent chord below the main wing. With a Reynolds number of 609,000, the angle of attack has been altered from (- 6° to 46°). The optimum slot width was 14.7 percent of the chord, and the best slot depth was 4 percent of the chord. They discovered a 41.5 % increase in lift.

A Clark Y-14 wing with a strongly cambered auxiliary airfoil that was 14.5 percent of the primary wing was tested in 1933 by Fred and Millard [2]. The researchers utilized a vertical wind tunnel with a diameter of 5 feet (1.524 meters). A small plate was used on both sides to link the auxiliary and primary wings. The position of the auxiliary airfoil was examined at 141 different places above and in front of the primary wing in his experiments auxiliary wing produced 1.81 maximum lift coefficients, which is 40 % higher than the Clark Y-14's without an auxiliary airfoil.

In 2007 Abdullah [2] conducted an experimental study on a low-speed, rectangular air tunnel with dimensions of 50 mm × 100 mm using five smooth-surfaced cylindrical pieces of different diameters 12.5, 15, 17, 35 and 37 mm, which caused blockage rates of 37 %, 35 %, 17 %, 15 % and 12.5 % and Reynolds number 7×10^3 to 5×10^4 and air velocity limits 10 to 20 m/s. The study proved that the clogging rate was 37 % and 35 %, which caused a decrease in the pressure coefficient around the models and a decrease in velocity distribution in the back area of the cylinders with an increase in the obstruction factor.

In 1975 Smith [3] made a theoretical study show that Leading edge gaps in airfoils regulate flow circulation on the primary element. A correctly constructed slot is positioned far enough from the wing such that each component forms its own boundary layer. As a result, the velocity on the main wing's surface is decreased, and the pressure peaks.

In 2013 Kapidzic [4] presented a strength study of hybrid composite-aluminum airplane constructions. Because metals are used in many major parts, the number of hybrid metal-composite parts is growing. Traditionally, such structures have been shunned as a viable alternative. They reviewed that the current tendency in airplane design is to use more fiber composites in the structural components.

In 2018 Ali et al. [4] conducted a simulation study on aircraft wings has shown that wing behavior is non-linear in nature. Lift-to-Drag ratio is dropped by 5.64 percent when the wing is considered a flexible structure.

Dynamic fluid-structure interaction study was carried out using a combination of CFD and CSD solver.

In 2019 Zakuan et al. [5] used ANSYS software to model the structural behavior of a three-dimensional wing. The deformation of the lifting surface structure has been observed and determined using static structural and modal analysis.in two different situations, one with spars and ribs and the other with only two ribs at the root and tip of the wing. The second example of the wing showed less deformation than the first case.

In 2010 Ghassan et al. [6] conducted a study regarding aviation airplanes. Estimated aerodynamic loads were applied to the wing using the finite element computing tool COMSOL. Then they demonstrated that the wing is the component that generates lift necessary for heavier-than-air flight.

Based on the survey above, the current paper aims to study and analyze the stress and aerodynamics aspects for a slotted wing composed of composite materials with the aid of fluid-structure interaction. This analysis has not been investigated intensively, thus this study contributes in more understanding such problems.

2. Mathematical descriptions

Using the Clark-Y 14 airfoil in Fig. 3 with slat and the Navier-stocks equation for 2D, unsteady state, incompressible, Newtonian fluid, and turbulent flow with constant fluid characteristics, and a composite wing of Carbon Epoxy with (1.6×10^3 kg/m^3) density, two layers arrayed in two directions (45°, - 45°).

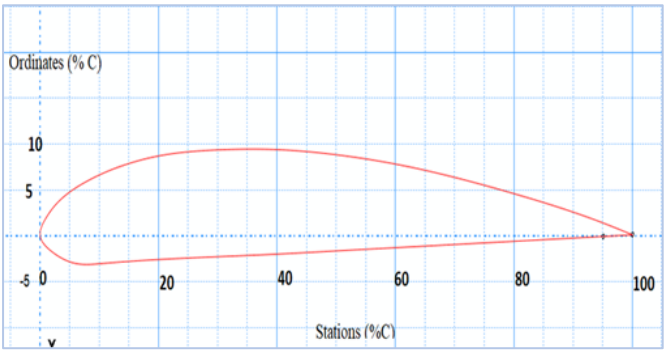

Fig. 3 Clark Y-14 airfoil.

The coordinates for the Clark-Y airfoil with slat only employed in this investigation are listed in Table 1 [1].

Table 1. The coordinates for the Clark-Y 14 airfoil with slat.

Auxiliary wing			Main wing			Main wing		
Stations	Ordinates		Stations	Ordinates		Stations	Ordinates	
From	Upper	Lower	From	Upper	Lower	From	Upper	Lower
Leading	Surface	Surface	Leading	Surface	Surface	Leading	Surface	Surface
edge			edge					
0	3.5	3.5	1.83	1.65	1.65	40	11.4	--
1.25	5.45	1.93	2.5	*2	1.47	50	10.51	--
1.85	--	1.63	5	--	0.93	60	9.15	--
2.5	6.5	*1	7.5	--	0.63	65	8.3	--
5	7.9	--	10	--	0.42	70	7.35	--
7.5	8.85	--	13	10.07	--	80	5.22	--
10	9.6	--	15	10.69	0.15	90	2.8	--
13	10.27	10.07	20	11.36	0.03	95	1.49	--
			30	11.7	--	100	0.12	--

Every dimension is a per cent chord.
*1 Use radius of 15 per cent chord from sta.1.85 to sta. 13 and corresponding ordinates.
*2 Use radius of 20 per cent chord from sat. 1.85 to sta. 13 and corresponding ordinates.

The governing equations are as below [6 - 9]:

Continuity Equation:

$$\frac{\partial u}{\partial x} + \frac{\partial v}{\partial y} = 0 \tag{1}$$

Momentum Equation in X-direction:

$$\frac{\partial U^2}{\partial x} + \frac{\partial UV}{\partial y} = -\frac{1}{\rho}\frac{\partial P}{\partial x} + \frac{\partial}{\partial x}\left(v\frac{\partial U}{\partial x}\right) + \frac{\partial}{\partial y}\left[v\frac{\partial U}{\partial y}\right] + \frac{\partial}{\partial x}\left(-\overline{\acute{u}^2}\right) + \frac{\partial}{\partial y}\left(-\overline{\acute{u}\acute{v}}\right) \tag{2}$$

Momentum Equation in Y-direction:

$$\frac{\partial UV}{\partial x} + \frac{\partial V^2}{\partial y} = -\frac{1}{\rho}\frac{\partial P}{\partial y} + \frac{\partial}{\partial x}\left(v\frac{\partial V}{\partial x}\right) + \frac{\partial}{\partial y}\left(v\frac{\partial V}{\partial y}\right) + \frac{\partial}{\partial x}\left(-\overline{\acute{u}\acute{v}}\right) + \frac{\partial}{\partial y}\left(-\overline{\acute{v}^2}\right) \tag{3}$$

U and V are the velocity components in X and Y directions where [8]:

$$U = \bar{U} + \acute{u}$$

$$V = \bar{V} + \acute{v}$$

$\partial P/\partial x$ and $\partial P/\partial y$ are pressure gradients, and the turbulent stresses:

$$-\overline{\acute{u}^2}, \qquad -\overline{\acute{v}^2}, \qquad -\overline{\acute{u}\acute{v}}$$

This can be expressed by the following formula if isentropic turbulence is assumed [9]

$$-\overline{\acute{u}^2} = 2\nu_t \frac{\partial U}{\partial x}$$

$$-\overline{\acute{v}^2} = 2\nu_t \frac{\partial V}{\partial y}$$

$$-\overline{\acute{u}\acute{v}} = \nu_t\left(\frac{\partial U}{\partial y} + \frac{\partial V}{\partial x}\right)$$

ν_t is the turbulent kinematic viscosity.

The k-ε turbulence model has been used for two dimensional Clark-Y wing. The turbulence kinetic energy K is the instantaneous kinetic energy k (t) of a turbulent flow. While the dissipation rate of (k) is known as (ε) [10]. This can be calculated as below:

$$\frac{Dk}{Dt} = \frac{\partial}{\partial x_j}\left(\frac{\nu_t}{\sigma_k}\frac{\partial k}{\partial x_j}\right) + P_k - \varepsilon \tag{4}$$

$$\frac{D\varepsilon}{Dt} = \frac{\partial}{\partial x_j}\left(\frac{\nu_t}{\sigma_\varepsilon}\frac{\partial \varepsilon}{\partial x_j}\right) + \frac{\varepsilon}{k}(C_{\varepsilon 1} P_k - C_{\varepsilon 2}\,\varepsilon) \tag{5}$$

$$P_k = \nu_t\left(\frac{\partial \overline{u_i}}{\partial x_j} + \frac{\partial \overline{u_j}}{\partial x_i}\right)\frac{\partial \overline{u_i}}{\partial x_j} \tag{6}$$

Where $C_{\varepsilon 1}$, $C_{\varepsilon 2}$, σ_k and σ_ε are the empirical parameters used in k-ε models and there values are: $C_{\varepsilon 1}$ = 0.09, $C_{\varepsilon 2}$ = 1.92, σ_k = 1.0 and σ_ε = 1.3.

The characteristics of air flow that used in this research are depicted in Table 2, where (ρ) is air density, (V) is the velocity input to the domain, (L) is chord length, and (μ) is dynamic viscosity of air and Reynolds number was calculated from the equation below:

$$Re = \frac{\rho V L}{\mu} \tag{7}$$

Table 2. characteristics of air flow.

Properties	Values	Units
Air density	1.2	kg/m^3
Dynamic viscosity	1.85×10^{-5}	Pa.s
Initial velocity	100	m/s
k-ε model paramter	0.09	-
Chord length	0.1	m
Reynolds number	6.49×10^5	-
Kinetic energy	13.5	Joule
Dissipation rate	1160	m^2/s^3

For the Fluid-Solid Coupling the solid equation was:

$$\rho_s \frac{\partial d_s}{\partial t} = \nabla \cdot \sigma_s + f_s \tag{8}$$

In the last equation ρ_s is the solid density, ds is the mesh displacement of the solid domain, σ_s is the tensor of Cauchy stress, and fs is the vector volume force.

Boundary Conditions

The domain section test we employed has a 220 mm width with and 100 mm height. In addition, the graphic depicts the border conditions stations. As indicated in Fig. 4.

1. Inlet section: inlet velocity is (100 m/s), turbulent flow then kinetic energy equal to (13.5 Joule) and dissipation rate (1.16×10^3 m^2/s^3).
2. Outlet section: pressure = 0.
3. At wall condition no slip.
4. Interface :

$$u = \frac{\partial d_{s,x}}{\partial t} \tag{9}$$

$$v = \frac{\partial d_{s,y}}{\partial t} \tag{10}$$

2.1. Lift and drag coefficients equations

Lift (L) is determined by the connection between the air density (ρ), the airfoil velocity (V), the wing surface area (S), and the coefficient of lift (C_L) in the equation below. Lift quickly reduces as the airplane reaches its maximum AOA called the $C_{L,MAX}$ critical AOA [11].

$$C_L = \frac{L}{\frac{\rho V^2}{2} \cdot S} \tag{11}$$

The coefficient of drag is dimensionless, it is often low at low AOA. Drag is used to measure how much an item drags in a fluid environment. It's always related with a certain surface area - D is for drag, ρ is for density.

$$C_D = \frac{D}{\frac{\rho V^2}{2} \cdot S} \tag{12}$$

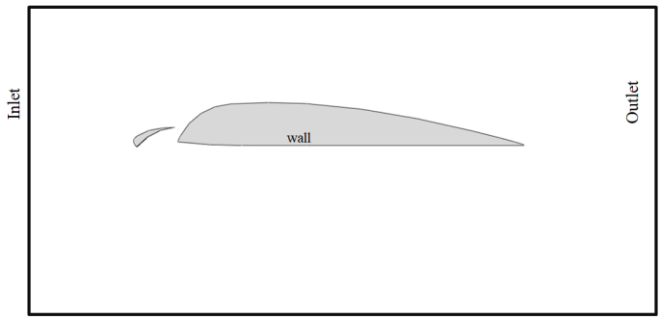

Fig. 4 Computational domain.

2.2. Performance coefficient

The performance coefficient C_E is a measure of how much lift and drag a streamlined surface can achieve with the least force impeding the wing. The obstruction coefficient has a distinctive role in determining the efficiency of smooth surfaces, as the highest efficiency can be obtained at the lowest obstruction force [11].

$$C_E = \frac{C_L}{C_D} \tag{13}$$

3. Numerical tool

It is useful to describe the numerical tool that is implemented in the present research, namely the finite element method. FEM is a numerical methodology that may be used to address issues in solid mechanics, fluid mechanics, heat transport, and vibrations. It is ideally adapted to digital computers. A CFD model of an airplane wing was created, which was surrounded by a fluid domain in 2D. A high cell density is essential to capture locations where separation occurs. The mesh density was chosen for these high situations in this investigation and then applied to all positions Fig. 5 [13], [14].

A solid is partitioned into a finite number of elements that are linked together at nodes. The displacements of each element in solid models are proportional to the nodal displacements. The strains and stresses in the elements are then linked to the joints' nodal displacements. Fig. 6.

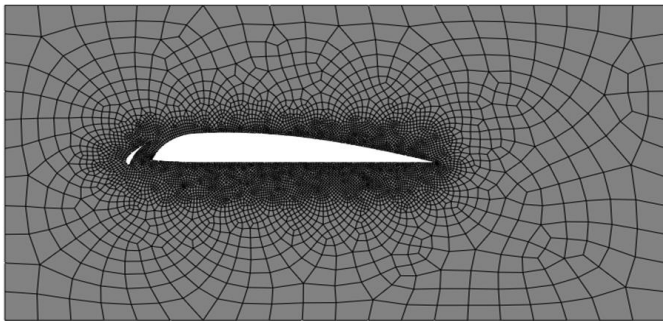

Fig. 5 Finite element for fluid domain.

Fig. 6 Finite element for solid domain.

3.1. ABAQUS multiphasic simulation

ABAQUS is an integrated environment for simulation application in a variety of disciplines and academic domains. It's also properly interfaced with most of the main CAE packages, which is a CAE Engineer's dream. The software was chosen for its great potential as well as its ability to meet research's objectives [15].

FSI is a category of Multiphysics issues in which fluid flow influences compliant structures, which in turn impacts fluid flow.

3.2. Mesh dependance test

A mesh independence test was performed to confirm that the size of the mesh had no influence on the solution and to investigate the effect of mesh quality on solution correctness. This was accomplished by comparing and contrasting six distinct grid arrangements' convergence behavior of velocity, pressure, and stress. Table 6 shows the number of elements and the values of velocity, pressure, and stress against every number of elements.

Table 3. elements number with velocity, pressure and stress.

Mesh	Elements	Velocity (m/s)	Pressure (Pa)	Stress (Pa)
G1	9876	1.38×10^2	4.30×10^3	1.52×10^5
G2	9979	1.37×10^2	4.23×10^3	1.45×10^5
G3	10199	1.37×10^2	4.24×10^3	1.48×10^5
G4	10249	1.37×10^2	4.22×10^3	1.78×10^5
G5	10444	1.38×10^2	4.29×10^3	1.85×10^5
G6	10473	1.38×10^2	4.34×10^3	1.96×10^5

The velocity was steady in the 6 values that were applied to the number of elements starting at 9876 and ending at 10473 elements, as shown in Fig. 7.

The same was true when it came to pressure. We can see that pressure is steady, but stress is stable in the range of elements from 9876 to 10199, then increases, but becomes practically stable between 10249 and 10473 elements.

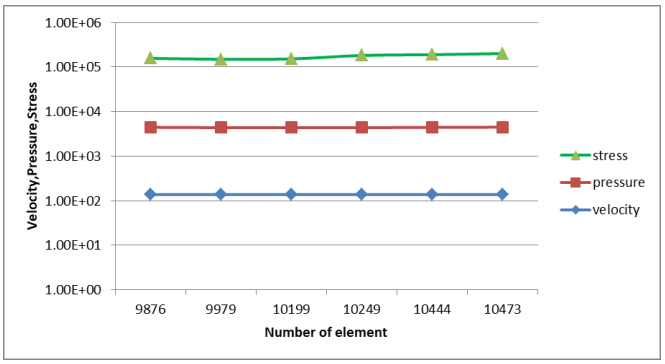

Fig. 7 Deviation in the values of velocity, pressure and stress with mesh size.

For more confidence in the used software, the computational model is validated by comparing the present result of C_L and C_D with the results presented by Abbas [16].

Table 4. A computational the present result of C_L and C_D with the results presented by Abbas [15].

Abbas						Present study	
EWT		JAVAFOIL		ANSYS			
C_L	C_D	C_L	C_D	C_L	C_D	C_L	C_D
1.4153	0.374	2.002	0.10587	1.5148	0.2861	1.43	0.13

4. Results and discussion

After all of the CFD and FSI simulations in the various slotted wing models were completed, the data was gathered into parts and studied separately. The lift, drag coefficients and stress curves of all the models are evaluated in this section by their distinctive components, such as maximum lift and drag coefficients.

In this research, fluid and Stress analysis was performed after the load and boundary conditions have been applied to the finite element model to determine pressure and velocity distribution and the greatest stress concentration area and compute lift and drag coefficient. We employed three different depths for the slat of an aircraft wing (d = - 3 %, 0 %, 4 %) of the chord, keeping the width (w = 13 %) and gap (g = 2.5 %) values fixed.

The output flow field variables such as pressure and velocity, as well as their distribution in the fluid domain, are displayed in the CFD results as seen in Figs. 7 and 8.

From the pressure distribution shown in Fig. 7, the following can be observed:

1. At the depth of – 3 % of chord and Reynolds number (6.49×10^5) the highest value of pressure comes at the front of the auxiliary wing and at the front of the main wing for a small area with a value of (6.209×10^3) Pa. This can be attributed to the fact of stagnation points that is the pressure get rises when the fluid is decelerated or completely stopped.
2. At the depth of 0 % of chord and Reynolds number (6.49×10^5) the highest pressure was concentrated in the front of the auxiliary wing with a larger area than the previous case. We note that it is concentrated in the front of the main wing and its value is (3.946×10^3) Pa and at the end of the main wing there is an appearance of a high-pressure value, but less than its maximum value is in the front where it is (1.078×10^8) Pa with an increase in the pressure value under the main wing.
3. At the depth of 4 % of chord and Reynolds number (6.49×10^5) we note that the pressure gradually increases towards the front of the slat until it reaches its highest value at the inner surface of the slat extending to the front of the main wing, where its value reached (4.155×10^3) Pa.

From the analysis of the figures that show the distribution of pressures, it can be noted that the highest-pressure value was at - 3% depth of the chord, which amounts to (6.209×10^3) Pa.

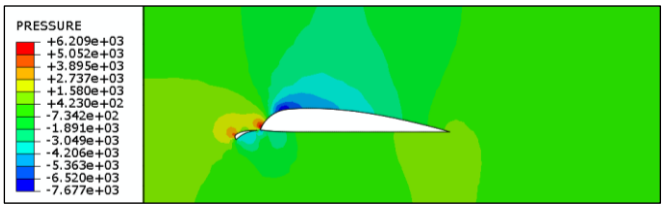

(a) Depth = - 3 %.

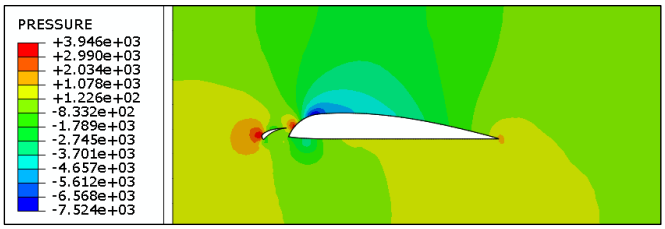

(b) Depth = 0 %.

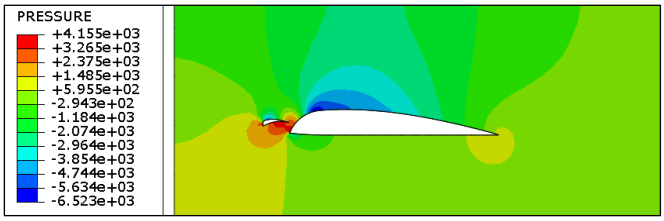

(c) Depth = 4 %.

Fig. 7 Pressure distribution in the fluid domain.

When examining Fig. 8 at Reynolds number (6.49×10^5), we notice the following:

1. In each of the two depths (- 3 %) and (0 %) from the chord we note that the highest value of the velocity was closely similar, as its value was (1.467×10^2) m/s and (1.46×10^2) m/s respectively, and it was centered on the upper surface. For the main wing within a small area above the layer in contact with the surface of the main and auxiliary wing, where the speed is the least possible and some points are equal to zero. This is because, at this depth, the tail of the airfoil is terminated with the leading edge of the main wing that provides a smooth path for air flow.
2. At the depth (4 %) from the wing chord, the maximum velocity is less than in the previous case, it became (1.337×10^2) m/s, but the area of its distribution on the upper surface is greater, while the surrounding path and contact with the surface of the wing remain less valuable and equal to zero in some points. This is due to the nature of the surface, as decreasing surfaces lead fluids to accelerate.

We can see that the highest velocity was obtained on the upper surface of the wing at the two depths (-3 percent) and (0 percent) of the chord, higher than at the depth (4 percent) of the chord. Although the highest value of the speed on the upper surface was less than the two preceding values, the velocity on the lower surface of the wing was greater than the previous two values.

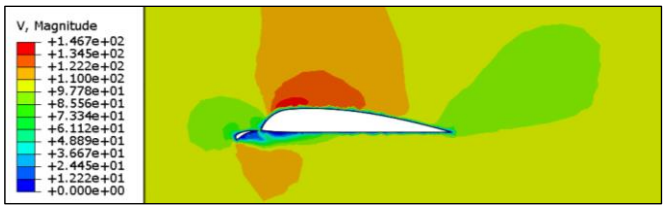

(a) Depth = - 3 %.

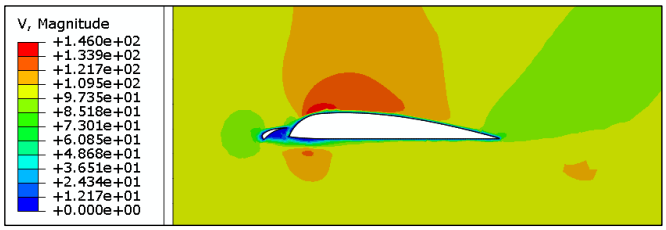

(b) Depth = 0 %.

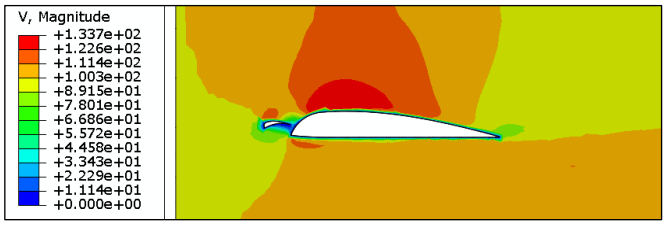

(c) Depth = 4 %.

Fig. 8 Velocity distribution in fluid domain.

In order to model and study the effects of real flight, dynamic fluid-structure interaction analysis is carried out. Fluid forces are passed to the structural module for structural analysis. The fluid forces caused stresses and deformation in the airplane wing, which were calculated. Maximum shear stresses and deformation were determined by a detailed investigation of Von-Mises stresses. The Fig. 9 below shows Von-Mises stress distribution:

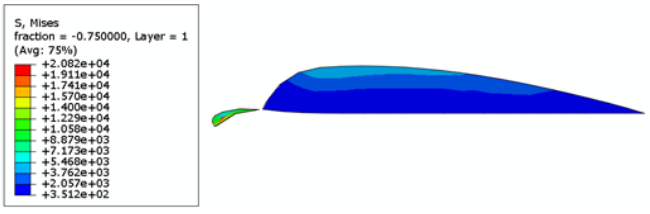

(a) Depth = - 3 %.

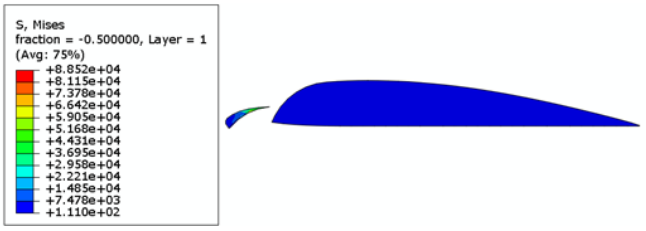

(b) Depth = 0 %.

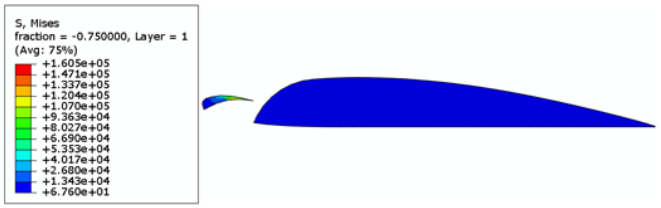

(c) Depth = 4 %.

Fig. 9 Von Mises stress distribution.

In Fig. 10 when the depth was (4 %), the maximum value of the fundamental stresses was in the direction of the *x*-axis (1.55×10^5) Pa and the lowest value was in the direction of the *x*-axis it measured (1.134×10^4) Pa at depth (- 3 %). In terms of the *y*-axis direction, the maximum value of stress was (5.82×10^3) Pa at depth (4 %) and the lowest value was (1.013×10^3) Pa at depth (- 3 %). In addition, the greatest values of shear stress in the *XY* and *YZ* planes at depth (4 %) were (1.143×10^4) Pa, while the lowest values were (2.73×10^3) Pa and (8.34×10^2) Pa, respectively in (- 3 %) that it can be clearly seen. Also, the relation between Von Misses stress and depth are represented in Fig. 10 where the greatest value of Von Misses stress was (1.605×10^5) Pa at depth (4 %) of the wing chord. The value of the Von Mises stress was calculated from the following equation [17]:

$$\sigma_v = \sqrt{\frac{(\sigma_{xx}-\sigma_{yy})^2+(\sigma_{yy}-\sigma_{zz})^2+(\sigma_{zz}-\sigma_{xx})^2}{2}+3(\sigma_{xy}^2+\sigma_{yz}^2+\sigma_{zx}^2)} \quad (14)$$

Table 5. Maximum stresses with different depths.

D %	σ_{xx}	σ_{yy}	σ_{xy}	σ_{zx}	Von Mises
- 3	1.23×10^4	1.01×10^3	2.73×10^3	8.34×10^2	20800
0	3.59×10^4	1.48×10^3	3.58×10^3	1.41×10^3	88500
4	1.55×10^5	5.82×10^3	1.14×10^4	1.14×10^4	161000

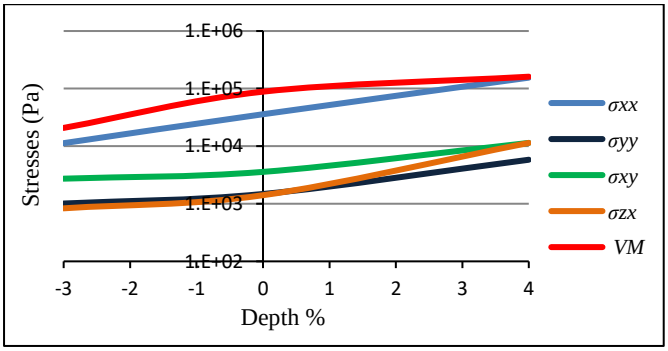

Fig. 10 Relationship between stresses and depth.

One of the important things to be obtained when designing any aircraft is to calculate or know the lift and drag coefficients because of their importance during take-off and landing, as the lift coefficient must be high at take-off and the drag coefficient is as low as possible, but in the case of landing, the opposite is true.

Therefore, we calculated both the lift and drag coefficients and plotted the relationship of each of them with the change in depth. In this research, we also calculated the performance coefficient from knowing each of the lift and drag coefficients and the relationship between them and then plotted the relationship of the performance coefficient with depth. Table 4 shows the values of each of them when all depth.

Table 6. Depth with lift, drag and performance coefficients.

D %	C_L	C_D	C_E
- 3	0.489	0.822	0.595
0	0.265	0.313	0.837
4	0.29	1.89	0.153

Figures 11-13 depict the relationship between these coefficients and depth:

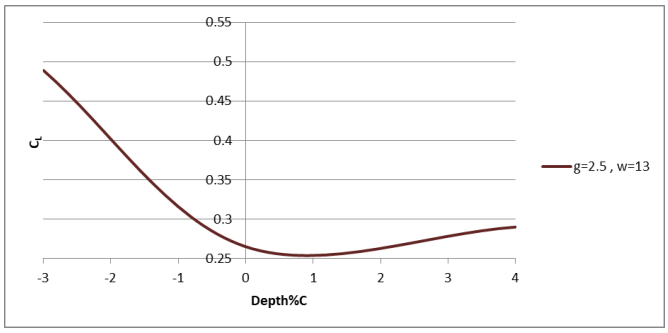

Fig. 11 Relation between C_L and depth.

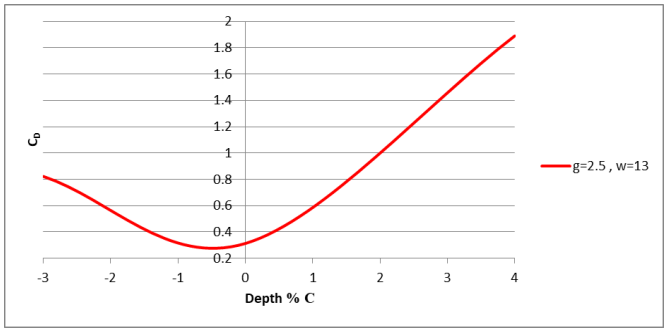

Fig. 12 Relation between C_D and depth.

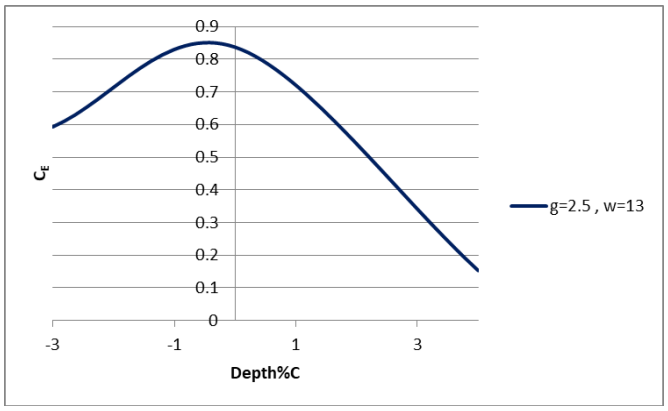

Fig. 13 Relation between C_E and depth.

Figure 11, which is illustrated by a curve, clearly shows the link between the lift coefficient and the slat depth. The lift coefficient has the largest value when the slat depth is equal to - 3 %, but it steadily falls as the depth approaches zero %, then returns to the height at depth 4 but with a value lower than that at depth - 3 %.

The relationship between the drag coefficient, which represents the fluid's obstruction of the wing structure, and the slat depth shows that the drag coefficient is lower at depth - 3 % than at depth 4, in contrast to the lift coefficient, and that as the curve approaches the zero point, i.e. at depth 0 %, the value of each lift and drag coefficient is very similar, as shown in Fig. 12.

Performance coefficient, which is the ratio of lift to drag, as a result of the presence of the lift and pull forces, through which the lift and drag coefficients were calculated, which represented graphically in Fig. 13, where it is clear that the highest ratio of the performance coefficient was at the depth 0 %.

4. Conclusions

A 2D slotted composite wing has been numerically simulated at a constant Reynolds number of (6.49×10^5) ABAQUS CFD and FSI for three wing designs basing on different depths revealed that:

1. By conducting a CFD simulation of the air-fluid and for three values of the depths of the slat as a percentage of the original wing chord, it was found that the highest pressure value was about the depth of - 3 % of the chord.
2. Through the simulation, different distributions of air velocity were also obtained for the three cases that were applied, where the value of the velocity at the depth 4 % of the wing chord was the lowest value with the largest impact area on the upper surface of the main wing.
3. The distribution of stresses on the structure of the composite wing was determined using FSI simulations. Small locations specified on the lower surface of the slat at a depth of 4 % of the wing chord had the greatest value of Von Mises stresses. The stresses on the main wing were constant between 0 and 4 percent depths, but at - 3 percent depth, the stress value ranged from 3.762×10^3 Pa to 3.512×10^2 Pa.
4. The focus is on more elastic structures where deformation and tension dissipate when external pressures are removed. Composites are made up of reinforced layers with appropriate resins and have a more aerodynamic look. As a result, the wing structure used in this article is made of carbon epoxy.
5. The highest value of the lift coefficient at depth is - 3 % for the slat, while the highest value of the coefficient of drag at depth is 4 % from the chord, and whenever the coefficient of lift is higher than the coefficient of drag, the performance coefficient is higher, but in present study, there was a convergence between the value of the coefficient of lift and drag at depth 0 %, where note that the value of the performance parameter at 0 % depth is the highest value.
6. The maximum value of Von Mises stress was found at depth of 4 % with value of 1.605×10^5 Pa.

Nomenclature		
Symbol	**Description**	**SI Unit**
C	Chord length	m
C_D	Drag coefficient	--
C_L	Lift coefficient	--
$C_{\varepsilon 1}.C_{\varepsilon 2}$	Turbulent empirical parameters	--
D	Drag force	N
k	Turbulent kinetic energy	m^2/s^2
L	Lift force	N
P	Pressure	N/m^2
Re	Reynolds number	--
S	Wing surface area	m^2
U, V	Mean velocities components	m/s
x, y	Cartesian coordinate	--
Greek Symbols		
Symbol	**Description**	**SI Units**
α	Angle of attack	degree
ε	Turbulent dissipation rate	m^2/s^3
μ	Air dynamic viscosity	kg/m.s
ρ	Air density	kg/m^3
$\sigma_k, \sigma_\varepsilon$	Constant for k-ε model	--
υ_t	Turbulent kinematic viscosity	m^2/s

References

[1] C. J. Wenzinger and J. A. Shortal, "The aerodynamic characteristics of a slotted Clark y wing as affected by the auxiliary airfoil position", NACA-TR-400, 1932.

[2] S. A. Yousif, "Effect of Wind Tunnel Blockage on Aerodynamics of Circular Cylinders", Basrah Journal for Engineering Science, Vol. 7, Issue 1, pp. 1-17, 2007. https://doi.org/10.33971/bjes.7.1.1

[3] A. M. O. Smith, "High-Lift Aerodynamics", Journal Aircraft, Vol. 12, No. 6, pp. 501-530, 1975.

[4] I. Ali, A. H. Memon, M. T. Bhatti, D. Kumar, I. A. Qazi, S. Banghwar, "Dynamic Fluid-Structure Interaction Analysis of Propeller Aircraft Wing", American Scientific Research Journal for Engineering, Technology, and Sciences (ASRJETS), Vol. 45, No. 1, pp. 64-74, 2018.

[5] M. A. M. B. M. Zakuan, A. Aabid, and S. A. Khan, "Modelling and structural analysis of three-dimensional wing", International Journal of Engineering and Advanced Technology (IJEAT), Vol. 9, Issue 1, pp. 6820-6828, 2019. https://doi.org/10.35940/ijeat.A2983.109119

[6] K. S. Mushatet, A. A. Ouda, and Q. A. Rishack, "Investigation of Non-Newtonian Fluids Flow Behavior in A Double Step Expansion Channel: Part 2", University of Thi-Qar Journal for Engineering Sciences, Vol. 9, No. 2, 2018. https://doi.org/10.31663/tqujes/9.2.301(2018)

[7] F. A. Naser and M. T. Rashid, "Effect of Reynold Number and Angle of Attack on the Hydrodynamic Forces Generated from A Bionic Concave Pectoral Fins", IOP Conference Series: Materials Science and Engineering, Vol. 745, No. 1, 2020. https://doi.org/10.1088/1757-899X/745/1/012026

[8] J. Burkardt, "Finite Elements for the (Navier) Stokes Equations", ISC 5939: Advanced Graduate Seminar, Department of Scientific Computing, Florida State University, 2011.

[9] Chapter 7 "An introduction to wing design", pp. 215-216.

[10] A. Bakker, "Lecture 10 - Turbulence Models Applied Computational Fluid Dynamics", Lecture Notes, No. 2002, pp. 1-47, 2006.

[11] Federal Aviation Administration, "Pilot's handbook of Aeronautical Knowledge: Aerodynamics of Flight", No. Cl, 2016.

[12] J. Kadim, F. A. Hamed, and H. Abdelwahhab, "The effect of aspect ratio and angle of attack on the aerodynamic performance of smooth surfaces", Damascus University Journal of Engineering Science, 2010.

[13] V. T. H. Hoang, "Simplified Design of a Commercial", 2015.

[14] B. K. S. Woods, J. H. S. Fincham, and M. I. Friswell, "Aerodynamic Modelling of the Fish Bone Active Camber Morphin", RAeS Applied Aerodynamics Conference, pp. 1-12, 2014.

[15] D. Systèmes, "Introduction to ABAQUS-CFD (fluid dynamics)", pp. 1-218, 2010. https://imechanica.org/files/CFD.pdf

[16] H. K. Abbas, "Investigation of New Slat Configurations on Clark Y-14 Wing for Enhancing Aerodynamic Performance", M.Sc. Thesis, Mechanical Engineering Department, College of Engineering, Al-Nahrain University, 2017.

[17] H. Dai, G. Chen, S. Li, Q. Fangb, and B. Hubc, "Influence of laser nanostructured diamond tools on the cutting behavior of silicon by molecular dynamics simulation", Royal Society of Chemistry, Vol. 7, pp. 15596-15612 2017. https://doi.org/10.1039/C6RA27070K